


1 Designing 3D RNA Origami Nanostructures with a 2 Minimum Number of Kissing Loops

3 Antti Elonen ✉ 

4 Department of Computer Science, Aalto University, Finland

5 Pekka Orponen ✉ 

6 Department of Computer Science, Aalto University, Finland

7 Abstract

8 We present a general design technique for rendering any 3D wireframe model, that is any connected
9 graph linearly embedded in 3D space, as an RNA origami nanostructure with a minimum number
10 of kissing loops. The design algorithm, which applies some ideas and methods from topological
11 graph theory, produces renderings that contain *at most one* kissing loop for many interesting model
12 families, including for instance all fully triangulated wireframes. The design method is already
13 implemented and available for use in the design tool DNAforge (<https://dnaforge.org>).

14 **2012 ACM Subject Classification** Theory of computation → Theory and algorithms for application
15 domains; Applied computing → Life and medical sciences → Computational biology

16 **Keywords and phrases** RNA origami, wireframe nanostructures, polyhedra, kissing loops, topological
17 graph embeddings, self-assembly

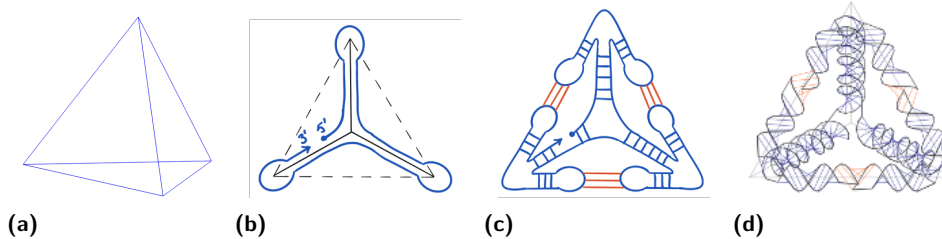
18 1 Background

19 Concurrently to the advances in DNA nanotechnology, there has been increasing interest in
20 using RNA as the fabrication material for self-assembling bionanostructures. In comparison
21 to DNA, the appeal of RNA is that the strands can be produced by the natural process
22 of polymerase transcription, and the structures can thus be created in room temperature
23 *in vitro*, and possibly eventually *in vivo*, from genetically engineered DNA templates. The
24 challenge, on the other hand, is that the folding process of RNA is kinetically more complex
25 and hence less predictable than DNA helix formation, at least at the present stage of RNA
26 engineering.

27 Starting from the mid 1990's, the leading design technique in this area of *RNA nano-*
28 *technology* has been “RNA tectonics”, whereby naturally occurring RNA structures are
29 connected together with connector motifs such as kissing-loop and sticky-end pairings,
30 to create complex target structures [11, 12]. A complementary top-down *de novo* design
31 approach of “RNA origami” was however presented in a landmark 2014 article by Geary
32 et al. [9]. In this method, broadly speaking, a given mesh model is rendered in RNA
33 by designing a strand that will, firstly, fold upon itself to realise a spanning tree of the
34 mesh by edges constituted as RNA helices, and secondly, induce the remaining edges by
35 kissing-loop motifs that connect matching half-edge hairpin loops at 180° angles to create
36 almost perfect “pseudo-helices”. (This abstract view in terms of mesh models and spanning
37 trees is from [16] and ignores many important details of the original work.) Following
38 article [9], which demonstrated the feasibility of the RNA origami design method by the
39 experimental synthesis and characterisation of several types of 2D RNA tiles, this line of
40 work has been further developed with new connector motifs, design techniques, and tools in
41 e.g. publications [15, 8].

42 Wireframe 3D RNA origami

43 The RNA origami idea has also been extended to cover 3D wireframe models [2]. (While
 44 article [2] addresses primarily polyhedral meshes, the method therein applies in fact to any
 45 connected straight-line wireframe model; that is, the meshes do not need to contain faces.)
 46 The basic spanning-tree based 3D design scheme is presented in Figure 1.



■ **Figure 1** A spanning-tree based design scheme for 3D RNA wireframe origami. (a) Targeted wireframe model. (b) A spanning tree and strand routing of the wireframe graph. (c) Routing-based stem and kissing-loop pairings. (d) Helix-level model. (Adapted with permission from [2].)

47 In this scheme, one starts from the targeted wireframe, which in the case of Figure 1(a)
 48 is a simple tetrahedron. (Or more precisely the wireframe skeleton of a tetrahedral mesh.)
 49 In the first design step (Figure 1(b)) one chooses some spanning tree T of the wireframe
 50 graph G , and designs the primary structure of the RNA strand so that it folds to create a
 51 twice-around-the-tree walk on T , covering each edge of T twice in antiparallel directions. In
 52 the second design step (Figure 1(c)) one then extends the walk halfway along each of the
 53 co-tree (= non-spanning tree) edges of G into a hairpin loop, and designs the base sequences
 54 at the termini of the hairpins so that pairwise matching half-edges connect to form the
 55 180° kissing-loop motifs mentioned earlier, thus constituting the co-tree edges. Figure 1(d)
 56 presents a helix-level model of the eventual nanostructure. (A similar design idea, although
 57 with different connector motifs and in the context of RNA-DNA hybrid nanostructures, has
 58 been recently applied also in the article [17].)

59 Challenges with kissing loops, goals of present work

60 Since the spanning tree of a connected graph with n vertices and m edges contains $n - 1$
 61 edges, its co-tree contains $m - n + 1$ edges, and this is the number of kissing-loop connections
 62 employed by the previous method. While the method thus in principle applies to all connected
 63 3D wireframe models, in practice using a large number of kissing-loop pairs in the designs
 64 raises some concerns. Firstly, kissing-loop pairings, which in the case of the 180° connector
 65 motif contain only six nucleotide pairs, may not be stable over long time scales. Secondly,
 66 the presence of a large number of slowly-forming tertiary structures such as kissing loops
 67 increases the risk of nonspecific pairings across structures, and hence aggregation of particles,
 68 in the synthesis stage. (There is some evidence of this in the experimental data presented
 69 in article [2].) And thirdly, there is at present no experimental data on large families of
 70 “orthogonal” kissing-loop pairs (high specific/low nonspecific pairing affinity) that would be
 71 needed for the design of complex structures using this method, and it is not even clear how
 72 large such families could reasonably be (cf. supplementary section S1.3.2. of article [2]).

73 Thus, in the present work we address the task of minimising the number of kissing loops
 74 in 3D RNA origami wireframe designs. As an application of an intimate connection between
 75 oriented strand routings on wireframes and topological graph embeddings, and building on

earlier work from different contexts [21, 6, 4], we derive a polynomial time strand-routing algorithm that goes beyond the simple twice-around-the-tree idea, and minimises the number of kissing-loop connections needed to complete the design. As it turns out, the minimum number of kissing loops needed is *at most one* for many interesting classes of models, including for instance all fully triangulated wireframes. The method is already implemented and easily accessible in the online design tool DNAforge [3].

In the following, Section 2 presents the tight connection between viable strand routings and graph embeddings, and Section 3 the ensuing kissing-loop minimising strand routing algorithm. Section 4 introduces some graph classes where the maximum number of kissing loops is at most one, Section 5 discusses the DNAforge tool, and Section 6 provides a summary and some notes on further research directions.

2 Strong antiparallel traces and topological graph embeddings

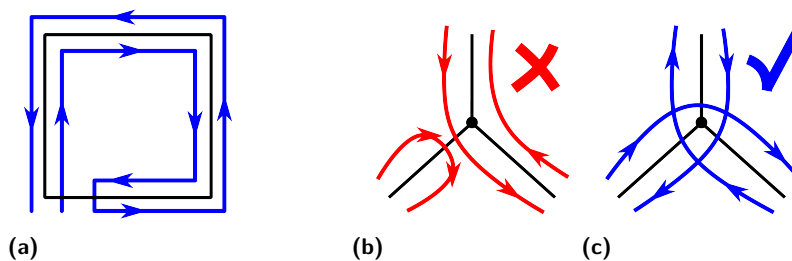


Figure 2 Strand routing criteria for RNA nanostructure design. (a) Edges covered twice in antiparallel directions. (b) Unstable vertex crossover pattern. (c) Stable vertex crossover pattern.

Let us first consider the possibility of rendering a given (connected) wireframe model using a single RNA strand with *no* kissing loops. This entails two conditions for the routing of the strand: firstly, every edge of the wireframe model must be covered twice, in antiparallel directions (Figure 2(a)); and secondly, the strand crossover pattern at each vertex must be *stable* (Figure 2(b)). The second condition signifies that if at a given vertex v with incident edges e_1, \dots, e_d , one considers edges e_i and e_j to be *locally coupled* when there is a strand segment that crosses from e_i to e_j or vice versa, then this local edge coupling (multi-)graph must be connected; and since by the first condition it is regular of degree 2, it must be a cycle. (In the literature, the local routing pattern of the strands at a vertex is called a “transition” in [5, 1] and the local edge-connectivity graph the “vertex figure” in [4].)

Thus, every viable RNA strand routing of a wireframe model corresponds to an antiparallel double trace of its edges, in such a way that the edge-to-edge crossings at each vertex follow some local cyclic order, viz. a cyclic permutation of the incident edges. As it turns out, these conditions are exactly equivalent to the respective abstract graph (that is, the model with geometry ignored) having a *1-face cellular embedding in some orientable surface*, a result established by Fijavž et al. in 2014, albeit in the context of polypeptide nanostructure designs [4]. Fijavž et al. call graph walks that satisfy the two indicated conditions *strong antiparallel traces*. (Earlier studies along the same lines, but not quite establishing the same connection, include e.g. [20, 19, 1, 13].)

Unfortunately, graphs that contain strong antiparallel traces are not that common, as observed already with an incomplete characterisation in [13]. Notably e.g. all of the Platonic solids are counterexamples, and thus cannot be properly rendered with a single RNA strand.

110 As we shall see, however, admitting even a single kissing loop in the designs changes the
111 situation dramatically.

112 Surfaces, graph embeddings, and Euler’s formula

113 To get a proper understanding of the methodology, let us review some key topology concepts
114 and results about surfaces and graph embeddings [14].

- 115 ■ A *surface* S is a topological space of dimension two (a 2-manifold), meaning that every
116 point in the space has a neighbourhood homeomorphic to an open unit disk. (A *homeo-*
117 *morphism* is a topological isomorphism, precisely speaking a continuous bijection between
118 two topological spaces with a continuous inverse.)
- 119 ■ A surface S is *orientable* if there is a consistent sense of clockwise/counterclockwise at
120 each point of S ; technically speaking if there is no embedding of the Möbius strip in S .
121 ■ We shall only be considering surfaces that are connected, orientable, topologically
122 compact and without boundary. This class of surfaces includes e.g. the sphere and
123 the torus, but not e.g. either the open disk (not compact) or the closed disk (has
124 boundary), and of course not nonorientable surfaces such as the Möbius strip or the
125 Klein bottle.
- 126 ■ From now on, the word “surface” in this paper means a connected, orientable, compact
127 surface without boundary, unless otherwise explicitly stated.
- 128 ■ The *genus* of a surface S is the number of nonintersecting cycles that can be drawn on S
129 without separating it.

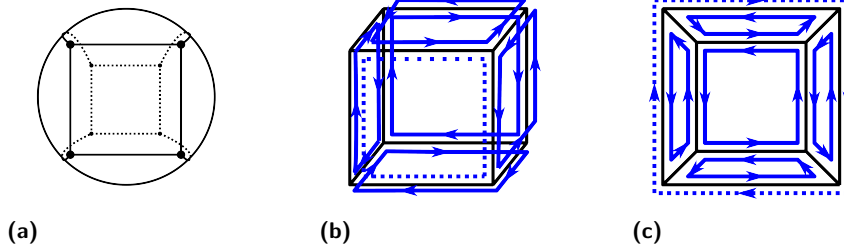
130 The classification theorem of surfaces states that every (connected, orientable, compact,
131 boundaryless) surface is homeomorphic to either the sphere or k torii sewn together (intuitively
132 the surface of a “ k -hole donut”), for some $k \geq 1$. Furthermore, since the sphere has genus 0
133 and a k -torus has genus k , for this family of surfaces the genus is a topological invariant:
134 any two surfaces with the same genus are homeomorphic, and vice versa.

- 135 ■ An *embedding* of a graph $G = (V, E)$ in a surface S is a continuous 1-1 mapping of G
136 into S as a system of points and arcs. (That is, the vertices V get mapped into points in
137 S , and the edges E into corresponding point-connecting arcs, in such a way that the arcs
138 don’t cross in S .)
- 139 ■ An embedding $\epsilon : G \rightarrow S$ divides S (or, technically, $S \setminus \epsilon(G)$) in disjoint *regions* or
140 *faces*. If every face is homeomorphic to an open disk, the regions are called *cells* and the
141 embedding is a *cellular embedding*.
- 142 ■ Any cellular embedding of a graph $G = (V, E)$ in a surface of genus g satisfies *Euler’s*
143 *generalised polyhedral formula*, or briefly just *Euler’s formula*:

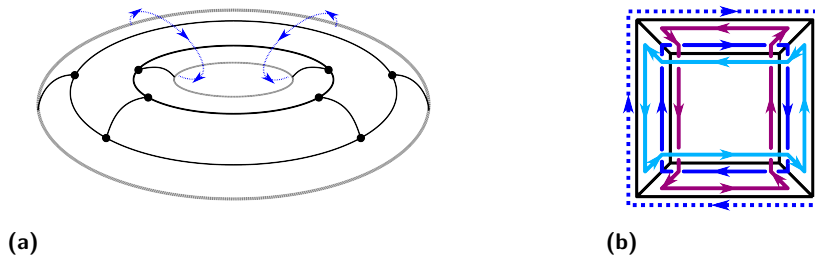
$$144 \quad |V| - |E| + |F| = 2 - 2g,$$

145 where $|F|$ is the number of cellular faces in the embedding.

146 To illustrate these concepts, let us consider the simple example of embedding the cube
147 graph. Figure 3(a) presents a “natural” cellular embedding of this graph in a sphere
148 surface. The embedding comprises six cells that correspond to the six faces of the 3D
149 cubical polyhedron. Figure 3(b) illustrates how the corresponding cubical wireframe could be
150 assembled using six RNA or DNA strands, each routing one of the faces of the cube cyclically
151 in a counterclockwise direction. (The strand that routes the front face is indicated separately
152 by a dotted line.) Figure 3(c) presents the same strand routing projected on the planar



■ **Figure 3** Cube graph embedded in a sphere surface. (a) Visualisation of the embedding. (b) Counterclockwise strand cycles routing the faces of the cube polyhedron model; each edge covered twice in antiparallel directions. (c) Faces and cycle routings presented in the Schlegel diagram of the model.

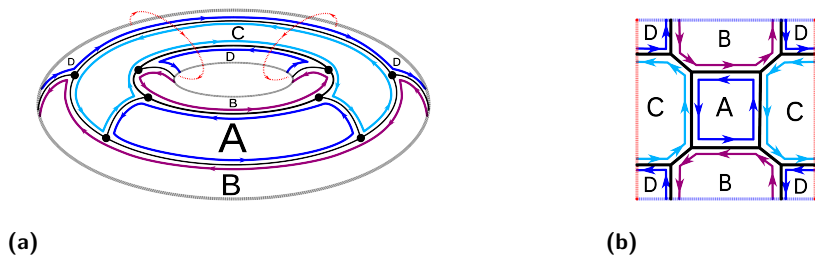


■ **Figure 4** Cube graph embedded in a torus surface. (a) Visualisation of the embedding. (b) Corresponding strand routings presented in the Schlegel diagram, with each edge covered twice in antiparallel directions.

153 *Schlegel diagram* of the polyhedron. Since the sphere has genus $g = 0$, one can validate that
 154 Euler’s formula holds: $|V| - |E| + |F| = 8 - 12 + 6 = 2 = 2 - 2g$.

155 However, the cube graph can also be cellularly embedded in a torus surface as presented
 156 in Figure 4(a). Now there are only four cells, and a corresponding system of four strands
 157 cyclically routing the cells, again in counterclockwise orientation and covering each of the
 158 graph edges twice in antiparallel directions, is outlined in the Schlegel diagram in Figure 4(b).
 159 For added clarity, Figure 5(a) indicates the four cells labelled as A, B, C, D, and Figure 5(b)
 160 shows the cell partitioning and the strand routings on a 2D torus diagram, which “folds around”
 161 at the top/bottom and left/right boundaries. Again Euler’s formula can be validated, now
 162 with the toroidal genus $g = 1$: $|V| - |E| + |F| = 8 - 12 + 4 = 0 = 2 - 2g$.

163 Note that in both of these cube graph embeddings, the strand crossovers at the vertices
 164 follow some cyclic order; in both cases actually the clockwise order around each vertex in the



■ **Figure 5** Cube graph embedded in a torus surface. (a) Labeled visualisation of the embedding. (b) Cell partitions and strand routings displayed on a torus diagram.

165 respective embedding surface. Conveniently, this arrangement (i) ensures that the vertices
 166 are *stable* in the sense defined earlier, and (ii) results in counterclockwise routes around the
 167 cells, which also guarantees that the cell boundaries, viz. the graph edges, are all covered
 168 twice in antiparallel directions.

169 In fact, any cellular embedding of a graph G in an orientable surface S induces such
 170 a system of (relative clockwise) permutations of incident edges at each vertex of G , that
 171 uniquely determines the embedding. And vice versa: any system of local edge permutations
 172 at the vertices of a graph G that also guarantees antiparallel coverage of the edges corresponds
 173 to some embedding in an orientable surface.

174 Note also that the number N of cyclic strands required to fabricate a graph $G = (V, E)$,
 175 or the corresponding metric wireframe, according to the recipe provided by a given cellular
 176 embedding equals the number of faces $|F|$ in that embedding. Thus, by Euler's formula, this
 177 number and the genus of the embedding surface are in an inverse relationship:

$$178 \quad N = |F| = |E| - |V| + 2 - 2g.$$

179 Thus, to minimise the number of strands needed, one should find an embedding into a surface
 180 of maximum possible genus. Ideally, one would hope to achieve $N = 1$, that is a cellular
 181 embedding in a surface of genus $g_{\text{ideal}} = \frac{1}{2}(|E| - |V| + 1)$ that comprises *a single face*. The
 182 cyclic strand route around this face would then constitute a strong antiparallel trace of the
 183 graph G .

184 **3 The Xuong tree design method**

185 As discussed earlier, many interesting graphs do not admit strong antiparallel traces, or
 186 equivalently single-face cellular embeddings of the absolutely maximum genus g_{max} . However,
 187 in the context of RNA origami design one can compromise on this target by judiciously
 188 removing some edges from the target graph G so as to reach the maximum *achievable*
 189 single-face embedding genus, and then reintroducing the removed edges as kissing loops. This
 190 is the idea underlying our *Xuong tree design method* for RNA origami, to be presented next.

191 Let $G = (V, E)$ be a connected graph, T a spanning tree of G , and $co(G, T) = G \setminus T$ the
 192 co-tree of G corresponding to T . All the spanning trees of G are of size (= number of edges)
 193 $|V| - 1$ and all the co-trees correspondingly of size $|E| - |V| + 1$. The latter value is called
 194 the *Betti number*, or cycle rank, of G .

195 The *Betti deficiency* $\xi(G, T)$ of a spanning tree T in G is defined to be the number
 196 of odd-sized components of $co(G, T)$. The *deficiency of a graph* G is the minimum Betti
 197 deficiency over all its spanning trees, $\xi(G) = \min_T \xi(G, T)$ [6, 21].

198 **► Theorem 1** (Xuong 1979 [21]). *The maximum achievable embedding genus of a graph G is*
 199 $\gamma(G) = \frac{1}{2}(\beta(G) - \xi(G))$.

200 [Note that, in reference to the previous section, $\gamma(G) = g_{\text{ideal}} - \frac{1}{2}\xi(G)$, hence the term
 201 “deficiency” $\xi(G)$.]

202 A spanning tree T^* that realises Theorem 1, that is for which $\xi(G, T^*) = \xi(G)$, is called
 203 a *Xuong tree*, and the maximum genus embedding of G can be found by constructing it
 204 around T^* in a process described in [21]. A fundamental operation in this process is inserting
 205 graph edges into faces, as represented by their boundary walks (= cycles in which edges
 206 may be repeated) in adjacent pairs. Consider two vertices, v_1 and v_2 . If v_1 and v_2 are along
 207 the boundary walk of a single face, adding a new edge between them results in the face,
 208 as represented by the walk, splitting in two (Figure 6b). Conversely, if v_2 and v_3 are not

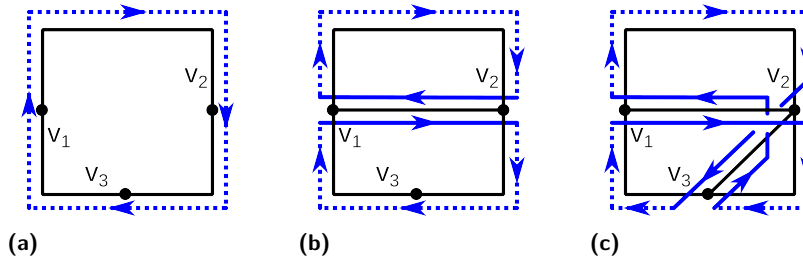


Figure 6 Splitting and joining faces by inserting edges. (a) A single face and its boundary walk. (b) The face/boundary walk is split in two by the insertion of an edge in the walk between vertices v_1 and v_2 . (c) The two faces/walks are merged into one with the insertion of another edge between v_2 and v_3 .

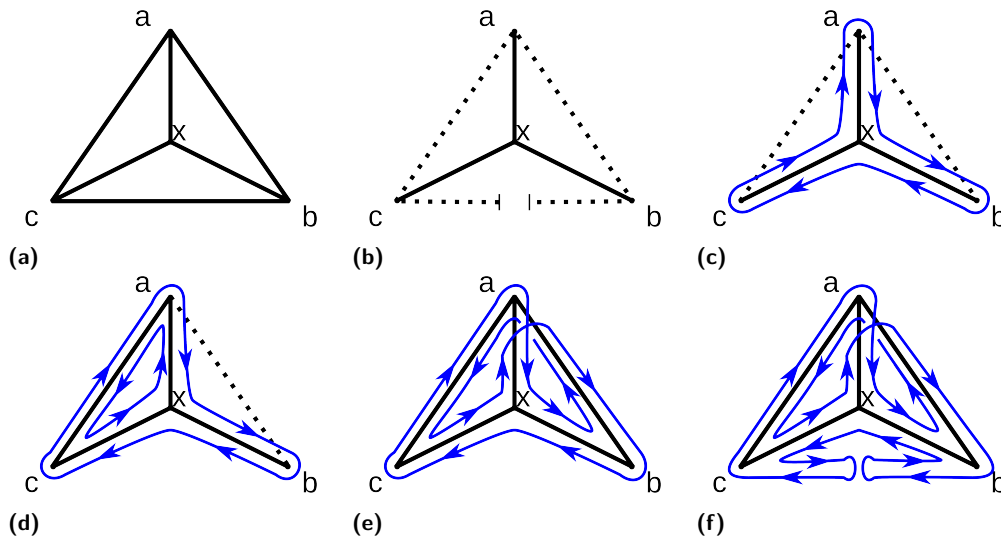


Figure 7 The Xuong-tree RNA wireframe design method applied on a tetrahedron. (a) A Schlegel diagram of a tetrahedron. (b) The tetrahedron with one edge removed and marked as a kissing loop. The solid line represents a Xuong tree. (c) The initial route along the Xuong tree: $a \rightarrow x \rightarrow b \rightarrow x \rightarrow c \rightarrow x \rightarrow a$ (d) The partial route augmented with a new edge $\{c, a\}$ from the co-tree. Note that the cycle count is now increased to two: $a \rightarrow x \rightarrow b \rightarrow x \rightarrow c \rightarrow a$ and $a \rightarrow c \rightarrow x \rightarrow a$. (e) After inserting the adjacent edge $\{a, b\}$, cycle count drops back to one: $a \rightarrow x \rightarrow b \rightarrow a \rightarrow c \rightarrow x \rightarrow a \rightarrow b \rightarrow x \rightarrow c \rightarrow a$ (f) The final tetrahedron with the deleted edge reintroduced as a kissing loop.

209 along the boundary walk of the same face, inserting an edge connecting them merges the
 210 two walks, i.e. faces into one (Figure 6c).

211 Since the boundary walk around a tree constitutes a single face, one can start with
 212 a 1-face embedding of T^* and then add two mutually adjacent edges from $co(T^*)$ to T^*
 213 and preserve the 1-face embedding. This process can be continued until all the even-size
 214 components in $co(T^*)$ are exhausted, and since T^* is specifically chosen to be a spanning
 215 tree of G such that $co(T^*)$ has the minimum number of odd components, a maximum genus
 216 embedding is found.

217 A Xuong tree T^* serving as a starting point for this process can be found in polynomial
 218 time by a reduction to the matroid parity problem for which polynomial time algorithms
 219 exist [18, 7]. This approach for finding Xuong trees was presented by Furst et al. [6], who also

220 provide a time complexity bound of $O(mnd \log^6 n)$ for the method, where m is the number
 221 of edges in the graph G , n is the number of vertices, and d the maximum vertex degree.

222 In case the graph G does not have a single-face embedding, it can be modified to have
 223 one by removing k edges, one edge for each odd component of $co(T^*)$. It is not possible
 224 to transform it into a single-face embeddable graph by removing any fewer edges than k .
 225 Suppose that removing $k - 1$ edges from G resulted in a single-face embeddable graph G_t . In
 226 that case, $\gamma(G_t) = \frac{2-|V|+|E_t|-|F_t|}{2} = \frac{2-|V|+|E|-k}{2} > \gamma(G) = \frac{2-|V|+|E|-|F|}{2} = \frac{2-|V|+|E|-k-1}{2}$,
 227 which is a contradiction, since G_t , a subgraph of G , cannot have a higher genus embedding
 228 than the highest genus embedding of G itself.

229 The Xuong tree design method routes the RNA strand around the single face embedding
 230 of the modified graph and replaces the removed edges with kissing loops. The number of
 231 kissing loops required is also minimised by the same argument as before. The Xuong tree
 232 design method is illustrated in figure 7 for a tetrahedron. Since a tetrahedron has 4 vertices
 233 and 6 edges, both all its spanning trees and co-trees have 3 edges, which means that any
 234 co-tree has at least one odd-sized component and a tetrahedron is not single face embeddable.
 235 (In fact all the co-trees of a tetrahedron are connected and of size 3.) By removing one edge,
 236 however, the tetrahedron can be 1-face embedded. The Xuong tree design method will then
 237 find a Xuong tree of the modified tetrahedron and use it to construct 1-face embedding. The
 238 removed edge is reintroduced as a kissing loop in the final step.

239 4 Upper embeddable graphs

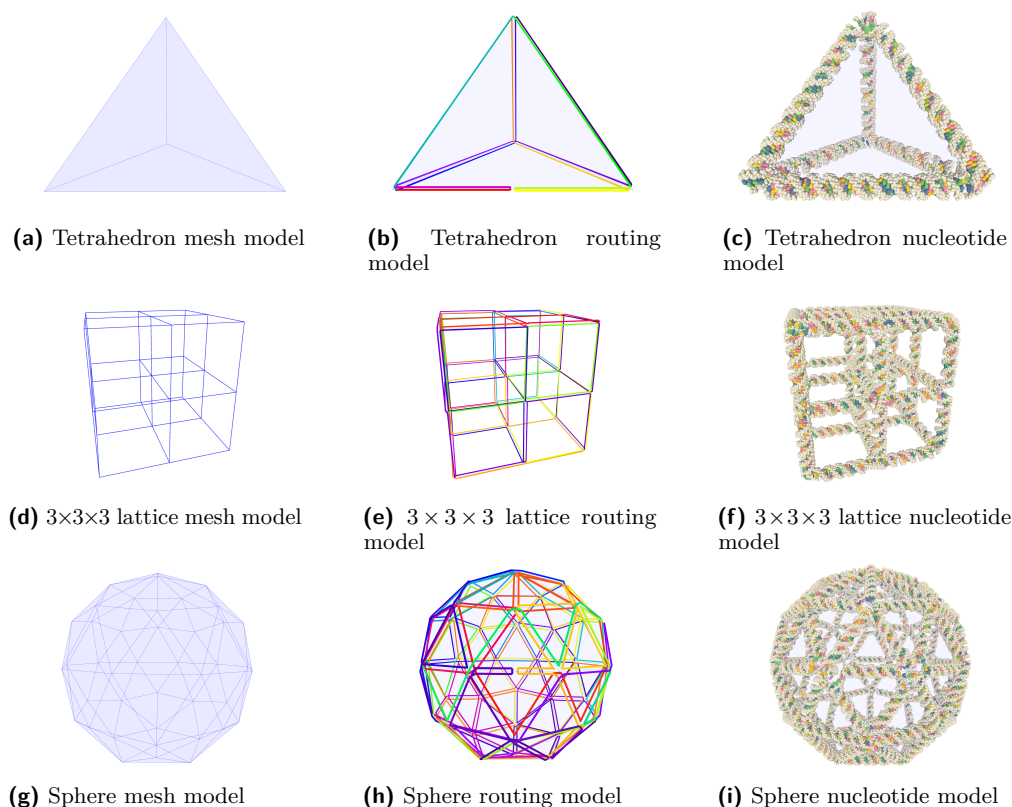
240 Graphs that readily admit a 1-face or a 2-face embedding are called *upper embeddable*. Such
 241 graphs require at most only one kissing loop using the Xuong tree design method. Many
 242 interesting graph classes are upper embeddable, including the following ones listed by Gross
 243 et al. [10, p. 752]

- 244 ■ Locally connected graphs,
- 245 ■ Cyclically edge-4-connected graphs,
- 246 ■ k -regular vertex-transitive graphs of girth g with $k \geq 4$ or $g \geq 4$,
- 247 ■ Loopless graphs of diameter 2,
- 248 ■ $(4k + 2)$ -regular graphs and $(2k)$ -regular bipartite graphs.

249 A graph G is *locally connected*, if for every vertex v in G , the open neighbourhood of v
 250 (vertices adjacent to v , excluding v) induces a connected graph in G . This graph class being
 251 upper embeddable is of particular interest, since it covers all fully triangulated polyhedra,
 252 e.g., tetrahedron, octahedron, icosahedron, and countless more. A graph G is said to be
 253 *vertex transitive*, if for every pair of vertices in G , there exists an automorphism mapping
 254 one vertex to the other. Intuitively, this means that the graph looks the same from the point
 255 of view of any individual vertex. All Platonic solids have this property, and, since cube and
 256 dodecahedron both have a girth (shortest cycle length) ≥ 4 , they too are upper embeddable.

257 5 The DNAforge design tool

258 DNAforge [3] is an online platform for designing DNA and RNA wireframe nanostructures
 259 from 3D models. The Xuong tree design method is integrated in DNAforge as XT-RNA. It
 260 allows users to transform any connected wireframe 3D model into a nucleic acid nanostructure
 261 with a single click. The workflow for the XT-RNA method is depicted in figure 8 for a
 262 tetrahedron, a $3 \times 3 \times 3$ cubical lattice, and a sphere. Note that the tetrahedron and the



■ **Figure 8** The XT-RNA design workflow in *DNAforge* for a tetrahedron ((a), (b), and (c)), a $3 \times 3 \times 3$ lattice ((d), (e), and (f)), and a sphere ((g), (h), and (i)).

263 sphere require only one kissing loop, presented in the foreground, whereas the lattice does
 264 not require any.

265 The DNAforge interface gives users options to minimise strain in the designed nanostructure
 266 via duplex-level physical simulation, or to simulate it directly from the interface with
 267 a nucleotide level simulation, provided the DNAforge backend is installed. The primary
 268 sequence is currently generated randomly, subject to Watson-Crick pairing conditions, and
 269 the routing is also currently found using randomised spanning trees instead of the matroid-
 270 reduction algorithm. In our experience, the randomised search works well, suggesting that
 271 typical graphs have many Xuong trees.

272 The final design can be exported as a PDB file, UNF file, or as OxDNA files, and the
 273 primary sequence can be exported as a CSV file.

274 6 Conclusion

275 Discussion and further work

276 We have introduced a general single-stranded RNA routing method, which minimises the use
 277 of kissing loops, and is based on high genus graph embeddings. The XT-RNA implementation
 278 is available at <https://dnaforge.org/>.

279 Note that even though the Xuong tree designs typically have at most only one kissing
 280 loop, the base pairing structure along the helices constituting the wireframe edges is highly

281 pseudoknotted. Development opportunities for the Xuong tree design method include
282 addressing the challenges posed by this pseudoknotted nature of its designs. These challenges
283 are related to the primary sequence generation and the knottedness of the actual nucleic
284 acid strands. While a strong antiparallel double trace of a wireframe model embedded on a
285 sphere-equivalent surface can be guaranteed to be an unknot, there are no such guarantees
286 for higher-genus wireframe models, and taking the helicity of RNA duplexes into account
287 will introduce knots even for the lower-genus models. These problems could potentially be
288 addressed by optimising the number and placement of kissing loops. Since RNA strands
289 are not closed cycles, however, the problem of knottedness might not be detrimental, and
290 practical experimentation is warranted.

291 ——— References ———

- 292 **1** Joanna A Ellis-Monaghan. Transition polynomials, double covers, and biomolecular computing.
293 *Congressus Numerantium*, 166:181, 2004.
- 294 **2** Antti Elonen, Ashwin Karthick Natarajan, Ibuki Kawamata, Lukas Oesinghaus, Abdulmelik
295 Mohammed, Jani Seitsonen, Yuki Suzuki, Friedrich C. Simmel, Anton Kuzyk, and Pekka
296 Orponen. Algorithmic design of 3D wireframe RNA polyhedra. *ACS Nano*, 16:16608–18816,
297 2022. doi:10.1021/acsnano.2c06035.
- 298 **3** Antti Elonen, Leon Wimbes, Abdulmelik Mohammed, and Pekka Orponen. DNAforge: A
299 design tool for nucleic acid wireframe nanostructures. *Nucleic Acids Research*, to appear. pre-
300 print: https://research.cs.aalto.fi/nc/papers/dnaforge_2024.pdf. doi:10.1093/nar/gkae367.
- 301 **4** Gašper Fijavž, Tomaž Pisanski, and Jernej Rus. Strong traces model of self-assembly poly-
302 peptide structures. *MATCH Communications in Mathematical and in Computer Chemistry*,
303 71:199–212, 2014. preprint: <https://doi.org/10.48550/arXiv.1308.4024>.
- 304 **5** Herbert Fleischner. *Eulerian Graphs and Related Topics. Part 1, Volume 1*, volume 45 of
305 *Annals of Discrete Mathematics*. North-Holland Publishing Co., Amsterdam, 1990.
- 306 **6** Merrick L. Furst, Jonathan L. Gross, and Lyle A. McGeoch. Finding a maximum-genus graph
307 imbedding. *Journal of the ACM (JACM)*, 35(3):523–534, 1988. doi: 10.1145/44483.44485.
- 308 **7** Harold N Gabow and Matthias Stallmann. Efficient algorithms for graphic matroid intersection
309 and parity. In *Automata, Languages and Programming: 12th Colloquium Nafplion, Greece,*
310 *July 15–19, 1985 12*, pages 210–220. Springer, 1985. doi:10.1007/BFb0015746.
- 311 **8** Cody Geary, Guido Grossi, Ewan K. S. McRae, Paul W. K. Rothmund, and Ebbe S. Andersen.
312 RNA origami design tools enable cotranscriptional folding of kilobase-sized nanoscaffolds.
313 *Nature Chemistry*, 13(6):549–558, 2021. doi:10.1038/s41557-021-00679-1.
- 314 **9** Cody Geary, Paul W. K. Rothmund, and Ebbe S. Andersen. A single-stranded archi-
315 tecture for cotranscriptional folding of RNA nanostructures. *Science*, 345(6198):799, 2014.
316 doi:10.1126/science.1253920. URL: [https://science.sciencemag.org/content/345/6198/](https://science.sciencemag.org/content/345/6198/799.abstract)
317 [799.abstract](https://science.sciencemag.org/content/345/6198/799.abstract), doi:10.1126/science.1253920.
- 318 **10** Jonathan L. Gross, Jay Yellen, and Ping Zhang. *Handbook of Graph Theory*. CRC Press, 2nd
319 edition, 2013.
- 320 **11** Peixuan Guo. The emerging field of RNA nanotechnology. *Nature Nanotechnology*, 5(12):833–
321 842, December 2010. doi: 10.1038/nnano.2010.231.
- 322 **12** Daniel Jasinski, Farzin Haque, Daniel W. Binzel, and Peixuan Guo. Advancement of the
323 emerging field of RNA nanotechnology. *ACS Nano*, 11(2):1142–1164, 2017. doi: 0.1021/ac-
324 snano.6b05737.
- 325 **13** Sandi Klavžar and Jernej Rus. Stable traces as a model for self-assembly of polypeptide
326 nanoscale polyhedrons. *MATCH Communications in Mathematical and in Computer Chemistry*,
327 70(1):317–330, 2013. url: <http://match.pmf.kg.ac.rs/content70n1.htm>.
- 328 **14** John Lee. *Introduction to Topological Manifolds*, volume 202. Springer Science & Business
329 Media, 2010. doi:10.1007/978-1-4419-7940-7.

- 330 **15** Di Liu, Cody W. Geary, Gang Chen, Yaming Shao, Mo Li, Chengde Mao, Ebbe S. Andersen,
331 Joseph A. Piccirilli, Paul W. K. Rothmund, and Yossi Weizmann. Branched kissing loops
332 for the construction of diverse RNA homooligomeric nanostructures. *Nature Chemistry*,
333 12(3):249–259, 2020. doi:10.1038/s41557-019-0406-7.
- 334 **16** Abdulmelik Mohammed, Pekka Orponen, and Sachith Pai. Algorithmic design of cotranscriptionally
335 folding 2D RNA origami structures. In *Unconventional Computation and Natural
336 Computation: 17th International Conference, UCNC 2018, Fontainebleau, France, June 25-29,
337 2018, Proceedings 17*, pages 159–172. Springer, 2018. doi: 10.1007/978-3-319-92435-9_12.
- 338 **17** Molly F. Parsons, Matthew F. Allan, Shanshan Li, Tyson R. Shepherd, Sakul Ratanalert,
339 Kaiming Zhang, Krista M. Pullen, Wah Chiu, Silvi Rouskin, and Mark Bathe. 3D RNA-
340 scaffolded wireframe origami. *Nature Communications*, 14(1):382, 2023. doi:10.1038/s41467-
341 023-36156-1.
- 342 **18** Matthias Stallmann and Harold N Gabow. An augmenting path algorithm for the parity
343 problem on linear matroids. In *25th Annual Symposium on Foundations of Computer Science,
344 1984*, pages 217–228. IEEE, 1984. doi:10.1109/SFCS.1984.715918.
- 345 **19** Carsten Thomassen. Bidirectional retracting-free double tracings and upper embeddability of
346 graphs. *Journal of Combinatorial Theory, Series B*, 50(2):198–207, 1990. doi:10.1016/0095-
347 8956(90)90074-A.
- 348 **20** Martin Škoviera and Roman Nedela. The maximum genus of a graph and doubly eulerian
349 trails. *Bollettino dell’Unione Matematica Italiana B*, 4 B:541–551, 1990.
- 350 **21** Nguyen Huy Xuong. How to determine the maximum genus of a graph. *Journal of Combinatorial
351 Theory, Series B*, 26(2):217–225, 1979. doi:10.1016/0095-8956(79)90058-3.